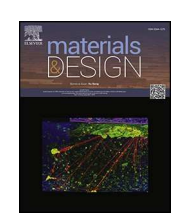
ELSEVIER

Contents lists available at ScienceDirect

Materials & Design

journal homepage: www.elsevier.com/locate/matdes





Conformal, stretchable, breathable, wireless epidermal surface electromyography sensor system for hand gesture recognition and rehabilitation of stroke hand function

Kerong Yang a,b , Senhao Zhang b,c,* , Ying Yang d , Xiaoman Liu d , Jiuqiang Li a,b , Benkun Bao a,b , Chang Liu a,b , Hongbo Yang a,b,* , Kai Guo a,b,* , Huanyu Cheng c,*

- a School of Biomedical Engineering (Suzhou), Division of Life Sciences and Medicine, University of Science and Technology of China, Hefei 230022, PR China
- ^b Suzhou Institute of Biomedical Engineering and Technology, Chinese Academy of Science, Suzhou 215011, PR China
- ^c Department of Engineering Science and Mechanics, The Pennsylvania State University, University Park 16802, USA
- ^d Department of Rehabilitation Medicine, The People's Hospital of Suzhou New District, Suzhou 215011, PR China

ARTICLE INFO

Keywords:

Epidermal sEMG sensor system Hand gesture recognition Rehabilitation of hand function

ABSTRACT

Surface electromyography (sEMG) plays a significant role in the everyday practice of clinic hand function rehabilitation. The materials and design of current typical clinic sEMG electrodes are rigid Ag/AgCl or flexible polyimide (PI) film, which cannot provide a stable interface between electrodes and skin for adequate long-term high-quality data. Thus, conformal, soft, breathable, wireless epidermal sEMG sensor systems have broad potential relevance to clinic rehabilitation settings. Herein, we demonstrate a stretchable epidermal sEMG sensor array system with optimized materials and structure strategies for hand gesture recognition and hand function rehabilitation. The optimized serpentine structures with marvelous stretchability and improved fill ratio, provide lower impedance and high-quality sEMG signals. Moreover, the easy-to-use airhole method further ensures stable and long-term contact with the skin for recording. In addition, integrated with a customized flexible wireless data acquisition system, the capability for real-time 8-channel sEMG monitoring is developed, and taking together with the CNN-based algorithm, the system can automatically and reliably realize the 7 kinds of hand gestures with an accuracy of 81.02%. Moreover, the low-cost yet high-performance epidermal sEMG sensor system demonstrated its conceptual feasibility in quantitatively evaluation of stroke patient's hand and facilitating human-robot collaboration in hand rehabilitation by proof-of-the-concept clinical testing.

1. Introduction

Stroke, as a major public health issue, has become the second leading cause of death and the primary cause of long-term disability [1], and the majority of stroke patients (\sim 75%) suffer functional movement disorder in their hands [2]. On account of the capacity for direct measurement of the hand function neuromuscular activity compared with the traditional single force evaluation through strain or force sensors, surface electromyography (sEMG) is a fundamental and comprehensive tool in the everyday practice of clinic hand function rehabilitation [3–9] (quantitative evaluation of patient [10], human–machine collaboration of rehabilitation equipment [11]). However, excessive pressure and medical tape to ensure stable skin-sensor interface contact of existing clinic

sEMG monitoring systems (i.e., fPCB-based sensors [12,13] or Ag/AgCl electrodes) still face the potential risks of iatrogenic skin injuries, meanwhile the poor skin-sensor interface also leads to higher impedance and lower signal-to-noise (SNR) ratio, which can't be ignored for clinic sEMG monitoring [14,15].

To date, recent advances in materials and biomedical engineering serve as the basis for sEMG sensors that have epidermal properties (mechanically bendable, stretchable, adhesive, and dynamically conform to human skin), allowing the collection of sEMG signals with high SNR [16–20]. There are two strategies to construct the epidermal sensors, one development of stretchable or reconfigurable sensors explores intrinsically stretchable conductive composites [17,21–23] or hydrogels [24], however, there are still challenges in integrating the

E-mail addresses: zhangsh@sibet.ac.cn (S. Zhang), yanghb@sibet.ac.cn (H. Yang), guok@sibet.ac.cn (K. Guo), huanyu.cheng@psu.edu (H. Cheng).

^{*} Corresponding authors at: Suzhou Institute of Biomedical Engineering and Technology, Chinese Academy of Science, Suzhou 215011, PR China (S. Zhang, H. Yang and K. Guo); The Pennsylvania State University, University Park 16802, USA (H. Cheng).

functional fPCB through a conventional soldering process to achieve extended signal processing and wireless capabilities for mass-production and commercialization. Alternatively, the stretchable metal structures (e.g., Au/Cr serpentine) with organic elastomer substrates (e.g., PDMS, Ecoflex) allow the conventional rigid metal to conform to contact with skin and is easy to use for building a comprehensive stretchable, wireless sEMG system [25-27]. Currently, further improvements and optimization of the widely used serpentine structure [28–31] are needed because of the lower fill factor (the area of the metal traces divided by the area of the electrode), resulting in lower skin-sensor contact impedance and a higher SNR. Additionally, the current fabrication of metal-film-based epidermal electrodes is the photolithography or "cut and paste" [32] method. Nevertheless, the complex process flow and extra chemical reagents pollution, as well as the limitation of large-scale pattern, make the photolithography challenging in actual application, and the "cut and paste" method struggles to meet the demand of sophisticated sensor pattern due to the employment of the mechanical cutter plotter. Meanwhile, some problems must be solved in clinic long-term applications such as breathability, and biocompatibility [33].

To the best of our knowledge, low-cost and efficient fabrication of epidermal sEMG sensor system is still lacking. Herein, we report a conformal, stretchable, breathable, biocompatible, wireless epidermal sEMG sensor system for hand gesture recognition and clinic hand function rehabilitation. An optimized design of serpentine structures was proposed to ensure sufficient stretchability and fill factor, allowing for enhancement of the skin-sensor contact impedance and improving the signal quality of sEMG. Additionally, the "laser cut and paste" method was conducted to manufacture the proposed sEMG sensors, which have the potential to be compatible with industrial "roll-to-roll" large-scale fabrication (Fig. 1a). As a result, the epidermal sensor with optimized structure and fabrication combines and exceeds the figure-ofmerits of hydrogels, fPCB-based electrodes, and epidermal electrodes with traditional serpentine and self-similar structures to open wider application opportunities (Fig. 1b). Moreover, customized flexible WiFibased wireless data acquisition electronics and software were integrated to demonstrate the capability of real-time 8 channels sEMG monitoring. Along with the proposed trained CNN algorithm, the seven-class hand gesture recognition related to hand function rehabilitation was achieved with high precision (~81.02 %). Furthermore, the proof-of-the-concept pilot study on stroke patients demonstrates the practical utility of the device for quantitative assessment of the patient's hands and human—machine collaboration of the custom-built hand rehabilitation robot (Fig. 1c).

2. Experimental section

2.1. Materials

A glass substrate (150 \times 150 mm) was purchased from GuLuoTM, China. PDMS kit (SYLGARDTM 184 Silicone Elastomer) was purchased from the Dow Chemical Company, USA. The Pyralux® copper/polyimide film (Cu/PI of 9 μ m/12 μ m) and PET film (200 μ m) were purchased from DuPontTM, USA. The water-soluble tape ASWT-2 was obtained from AquasolTM, Australia. Ecoflex 0030 (Part A and B) and release agent Ease Release®200 were purchased from Smooth-On, USA. The Silbione RT Gel4317 A/B was obtained from the ElkemTM, USA. The Anisotropic Conductive Film ANISOLM® AC-2056R was purchased from HitachiTM, Japan. Other chemical agents are purchased from Alfa Aesar. All electronic components are obtained from MouserTM, USA.

2.2. Fabrication

2.2.1. Fabrication of epidermal sEMG sensors ("Laser cut and paste" method)

The low-cost fabrication of the optimized epidermal sEMG sensor (Fig. S2) can be divided into the following three parts:

(i) Copper/polyimide film patterning ("Laser cut").

The transparent glass substrate was cleaned by isopropanol (IPA) first, and a mixture of base and curing agent in a weight ratio of 20:1 for polydimethylsiloxane (PDMS) precursor was spin-coated at 500 rpm for 20 s on a glass plate and cured at 90 °C for 20 min to form the sacrificial substrate. A layer of copper/polyimide film was laminated onto the cured PDMS surface. The designed epidermal sEMG sensors pattern by AutoCAD file was cut by a 355 nm UV laser at a pulse frequency of 50 kHz and a speed of 300 mm/s through a total of 9 times repeated cutting. It should be noted that the excess part near the pattern was directly removed by the laser to ensure that the remaining parts were connected and could be manually removed at once (Fig. S11).

(ii) Preparing breathable elastomer substrate.

After laminating a layer of double-sided tape on the glass plate, and a

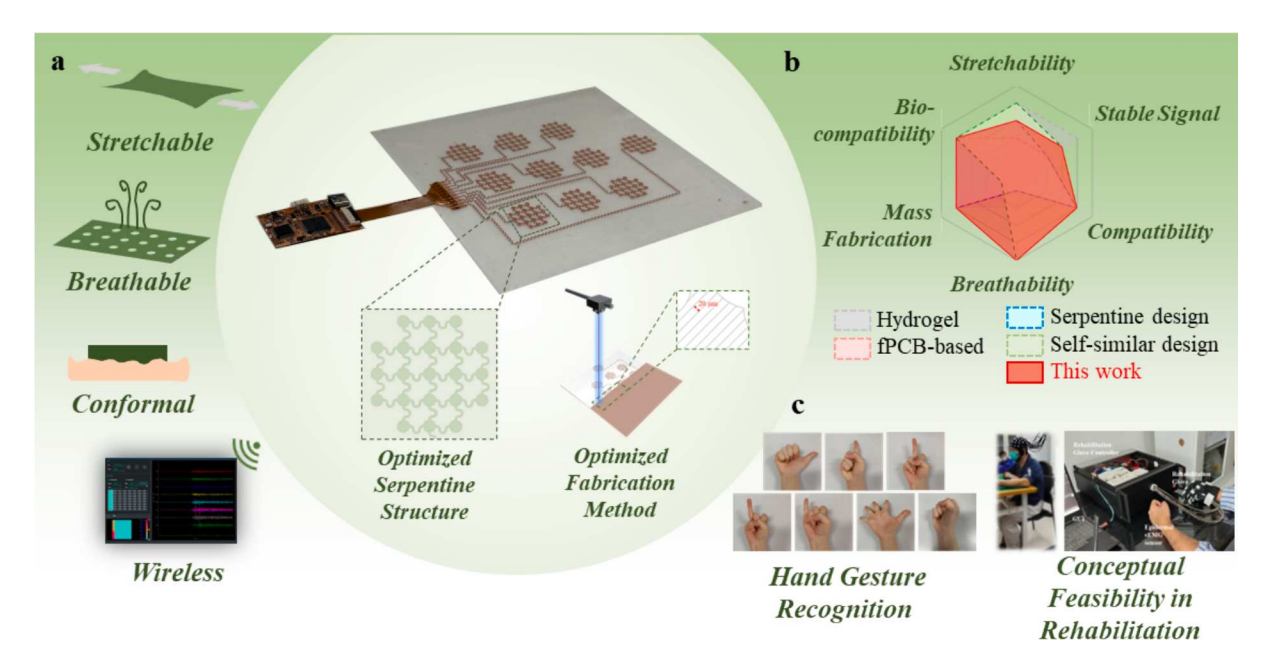


Fig. 1. The schematic illustrating the conformal, soft, breathable, wireless epidermal sEMG sensor system and application for hand gesture recognition rehabilitation of stroke hand function.

polyethylene terephthalate (PET) film was adhered to the double-sided tape. Then, a mixture of Ecoflex elastomer in a weight ratio of 1:1 (partA: partB) was spin-coated at 500 rpm for 20 s on the glass plate and cured at room temperature for 1 h. Silbione Gel4317 was spin-coated on the cured Ecoflex elastomer with a speed of 500 rpm for 20 s, followed by curing at 120 $^{\circ}\text{C}$ for 20 min. Moreover, the airholes were fabricated by the 50 W-CO₂ laser with raster mode at a power of 6.4 W and a speed of 40.89 mm/s to form the breathable elastomer substrate.

(iii) Transfer printing ("Paste").

The pattern formed by the "laser cut" part was picked up from the PDMS surface using water-soluble tape and transferred onto the breathable elastomer substrate. After dissolving the water-soluble tape with deionized (DI) water for 3 min to form the epidermal sEMG sensor.

2.2.2. Integration between recording system and epidermal sEMG sensors

The recording system and sensor-system connectors (SSC) were made by polyimide flexible printed circuit (FPC), and the electrical components of the recording system were soldered on the FPC according to the circuit design (Fig. S6). The SSC was designed and fabricated (EasyEDA, China) for connecting epidermal sEMG sensors. The SSC, ACF tape, and epidermal sEMG sensors were hot-pressed with a force of 40 N and temperature of 150 °C for 30 s by a hot-press machine (GZC-MS200, Hailunda, China). With a customized back-end connector, every channel of the epidermal sEMG sensor can be independently connected to the EMG recording system.

2.3. Characterization and algorithm model construction

2.3.1. FEA of mechanical properties

The commercial software ABAQUS (ABAQUS Analysis User Manual 2010, version 6.10) was employed for the determination of strain distribution (ϵ) in the stretchable copper foil structure of the sensor under tensile and bending deformations. Both the elastomer substrate layer and conductive electrodes layer of the sensor were modeled using hexahedral elements (C3D8R). The model consisted of approximately 3×10^5 elements and the mesh refinement was carried out to ensure convergence. The material properties of the electrodes were specified as Cu, with an elastic modulus (E) and Poisson's ratio (ν) of $E_{Cu}=119$ GPa and $\nu_{Cu}=0.34$, respectively. The flexible base layer was modeled using Ecoflex, employing an isotropic Mooney-Rivlin material model with parameters (C10 = 0.008054, C01 = 0.002013, D1 = 2).

2.3.2. Characterizations of the water-vapor transmission and peel force of the elastomer substrate

Based on ASTM E96 standards, water–vapor transmission rates were calculated by measuring the weight loss of water every 12 h by attaching the sample to seal the opening of a bottle with pure water.

Based on ASTM D3330 standards, 90° peeling tests were used to evaluate the peel force of the elastomer substrate by using a customized universal testing machine (M230pro, YiGao) (Fig. S12). The elastomer was attached to the volunteer's forearm skin, and with a stretching speed of 500 mm/min, the peel force was recorded by the force sensor.

2.3.3. Characterizations of the electronic property of the electrode

The skin-contact impedance of these electrodes (serpentine electrodes, optimized serpentine electrodes, traditional Ag/AgCl electrodes) was measured based dual-electrode method by using an electrochemical workstation (CHI660E, ChenHua) over a frequency range from 1 to 10^5 Hz at a voltage of 100 mV. Two electrodes were placed on the forearm with a separation of 50 mm. The EMG signals measured by these electrodes were recorded by the commercial data acquisition hardware (PowerLab, AD instruments) with a sample rate of 1000 Hz, and the SNR values were calculated with a 2 s window size using the following equation:

$$SNR(dB) = 20 log_{10} \times \frac{A_{signal}}{A_{noise}}$$

where the A_{singal} and A_{noise} mean the mean absolute value (MAV) of the signal and noise.

Furthermore, the signal-to-motion artifact ratio (SMR) is mainly used to quantitatively assess motion artifacts and is calculated as follows [34]:

$$SMR = \frac{P_{signal}}{P_{0-20 \text{ Hz}}}$$

The signal-to-high-frequency noise ratio (SHR) is mainly used to quantify high-frequency noise and is calculated by the formula [34]:

$$SHR = \frac{P_{signal}}{P_{upper20\%}}$$

where P_{signal} denotes the activation signal power, $P_{0\cdot 20~Hz}$ denotes the sum of the power densities of the activation signals below 20 Hz, and $P_{upper20\%}$ denotes the sum of the power densities of the activation signals at the higher 20 % of the frequencies.

2.3.4. In vitro evaluation of cell biocompatibility

A549 cells were cultured in serum-free medium (RPMI-1640, USA) supplemented with sterile-filtered L-glutamine, 100 units/mL penicillin, 100 µg/mL streptomycin (Penicillin Streptomycin, USA), and 0.1 g of the elastomer. The cultivation was carried out at 37 $^{\circ}\text{C}$ in an environment with 5 % CO₂ humidity. Subsequently, cell viability was observed under a microscope at 0, 18, and 24 h.

2.3.5. Machine learning and CNN classification model building

We utilized the epidermal sensor to acquire a 7-class gesture recognition dataset. The data collection took place in an indoor environment with 5 healthy adults as the participants. The experiment involved capturing 7 gesture actions, including thumb extension, index finger extension, middle finger extension, ring finger extension, little finger extension, five-finger open, and gripping. A total of 4050 gesture examples were collected, each consisting of an 11 s time series sampled at 500 Hz (window size: $11 \times 500 = 5500$ samples).

Several data preprocessing steps were undertaken to prepare the gesture recognition data. Initially, we applied a 50 Hz notch filter and a 10 Hz high-pass filter to the raw data. Subsequently, we standardized the time series data by scaling the amplitudes to a range between 0 and 1, with 80 % allocated to the training set and 20 % to the testing set. Labels indicated the gesture category corresponding to each sample, with a total of 7 gesture categories. Finally, we employed a CNN for gesture recognition.

The CNN architecture comprised multiple convolutional layers, specifically 9 convolutional layers, each consisting of a convolution operation and a ReLU activation function, followed by two fully connected layers. Dropout layers (p = 0.5) were added between the fully connected layers to mitigate overfitting risks. The parameters of the convolutional and fully connected layers were initialized using the Xavier initialization method, contributing to the stability and convergence of model training. The training process of the network involved the Adam optimizer and cross-entropy loss function for supervised learning. The learning rate was set to 0.001, with a batch size of 64 and the inclusion of L2 regularization. These hyperparameter values were chosen to enhance the model's convergence speed and generalization performance. The model's performance, including the confusion matrix and ROC curve, was evaluated on the test set to determine its classification accuracy across different gesture categories.

2.4. Clinical experiment

2.4.1. Experiment involving human participants

The human subject study was approved by the Medical Ethics Committee of The People's Hospital of Suzhou New District (Approval No. 2023-141). All human subjects gave written and informed consent before participation in the studies.

3. Results and discussion

3.1. Overall design, material, and fabrication strategies for epidermal sEMG sensors

There are three key functional layers of the 8 channels epidermal sEMG sensor as shown in Fig. 2a, the conductive metal trace layer (Cu/ PI, 9 μ m/10 μ m) is in direct contact with skin, which consists of 10 optimized serpentine electrodes (Fig. 2a-ii) (8 working electrodes, a

ground electrode, and a reference electrode) connected by filamentary serpentine wires (Fig. 2a-iii) (400 μm width), and the 10-pin flexible cables (Fig. 2a-iv) endow the sensors capacity of integrating external data acquisition and wireless transmission electronics. It's important to note that the coating of polyimide (PI) under the Cu-based wires provides mechanical strain isolation while enhancing the bonding force with silicone elastomer to avoid excessive out-of-plane strain. Additionally, an adhesive layer (Silbione RT Gel 4317, Elkem, 166.28 \pm 15.65 μm) and an ultra-thin support layer (Ecoflex-0030, 159.625 \pm 2.40 μm) compose the elastomer substrate. The adhesive layer provides weaker but robust bonding strength (peel adhesion of 0.89 N per 2.5 cm) with skin for long-term wear compared with traditional acrylic-based medical adhesives. Meanwhile, a removable PET sheet is always utilized to facilitate the manual manipulation of human skin (Fig. S1).

The "laser cut and paste" fabrication of epidermal sEMG sensors starts with the patterning of the conductive metal trace layer with a UV laser (LM-UV-3, DeLong) (Fig. 2b and Fig. S2). The pattern was followed

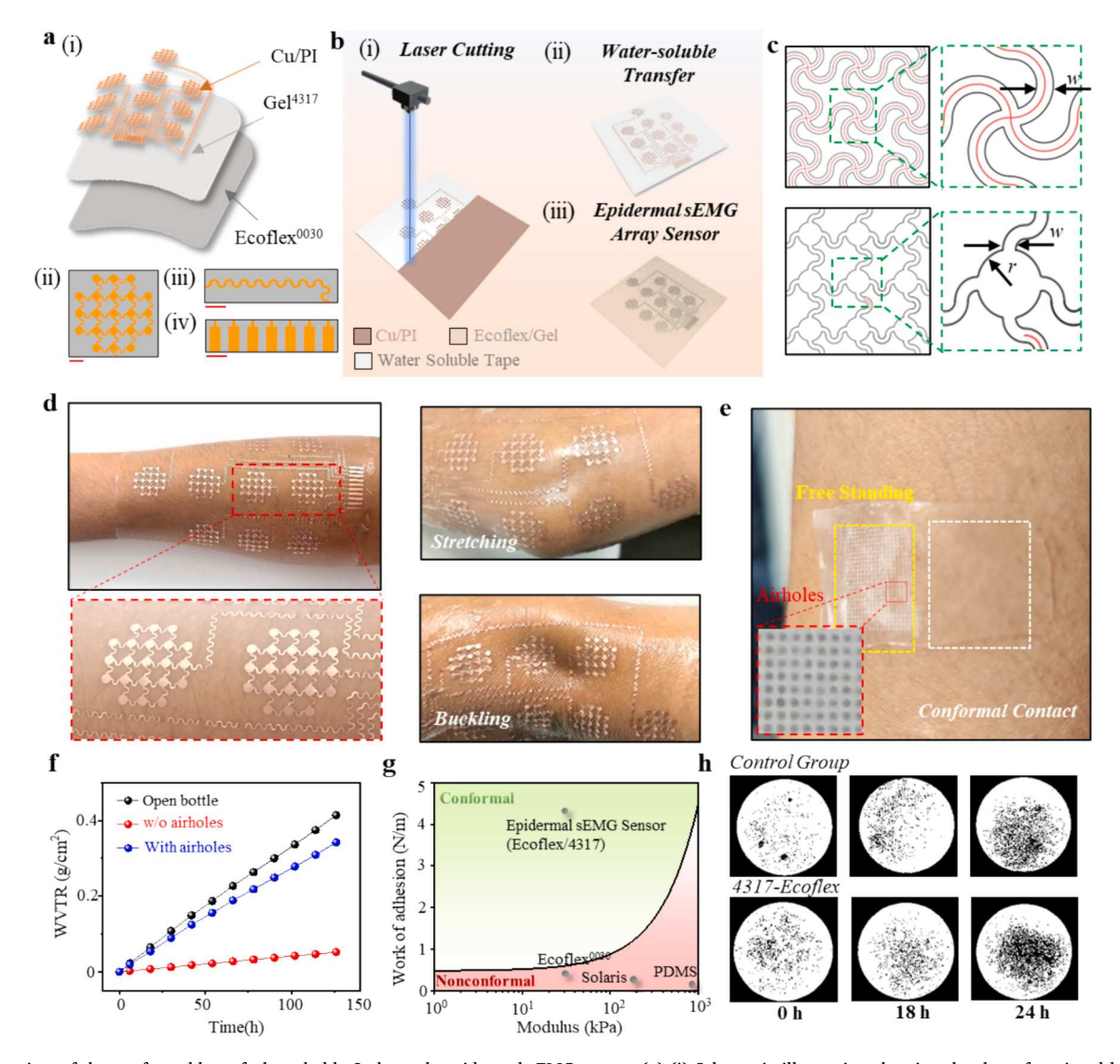


Fig. 2. Overview of the conformable, soft, breathable 8 channels epidermal sEMG sensor. (a) (i) Schematic illustration showing the three functional layers of the epidermal sEMG sensors. Diagrams of the (ii) optimized stretchable serpentine structure for EMG electrode (Scale bar, 3 mm), (iii) stretchable connect wires (Scale bar, 2.5 mm), and (iv) cables (Scale bar, 2.5 mm). (b) Fabrication process of the "laser cut and paste" for epidermal sEMG sensors. (c) Schematic illustration of the epidermal electrode with optimized serpentine design. (d) Photo of an epidermal sEMG sensor showing the conformable and soft property for direct lamination with the skin without other adhesives, and optical images of the epidermal sEMG sensor contact with skin during various mechanical deformations upon stretching and buckling. (e) Photography of Ecoflex0030/Gel4317 elastomer substrate with airholes attached to human skin. (f) Water vapor transmission range of the elastomer substrate with and w/o airholes, and open bottle. (g) Determination of conformal contact: The dotted curve represents the critical contact points of 300 μm thick elastomers. (h) Optical microscopy images of the human lung fibroblast cells cultured with Ecoflex0030/4317 for 18 h, and 24 h.

K. Yang et al. Materials & Design 243 (2024) 113029

by water-soluble transfer processing from the PDMS sacrificial layer to bonding with the new elastomer substrate (Ecoflex/4317). As shown in Fig. S3, the energy release rate (G) is crucial for the transfer processing, the pattern can successfully pick up from PDMS due to the G at the

interface of water-soluble tape (WST) and pattern ($G_{WST/Cu}$) is greater than the interface of PDMS and pattern ($G_{PDMS/Cu}$), and then the pattern with WST was laminated on the received elastomer substrate, and the $G_{WST/Cu}$ can suddenly disappear with the dissolution of WST, allowing

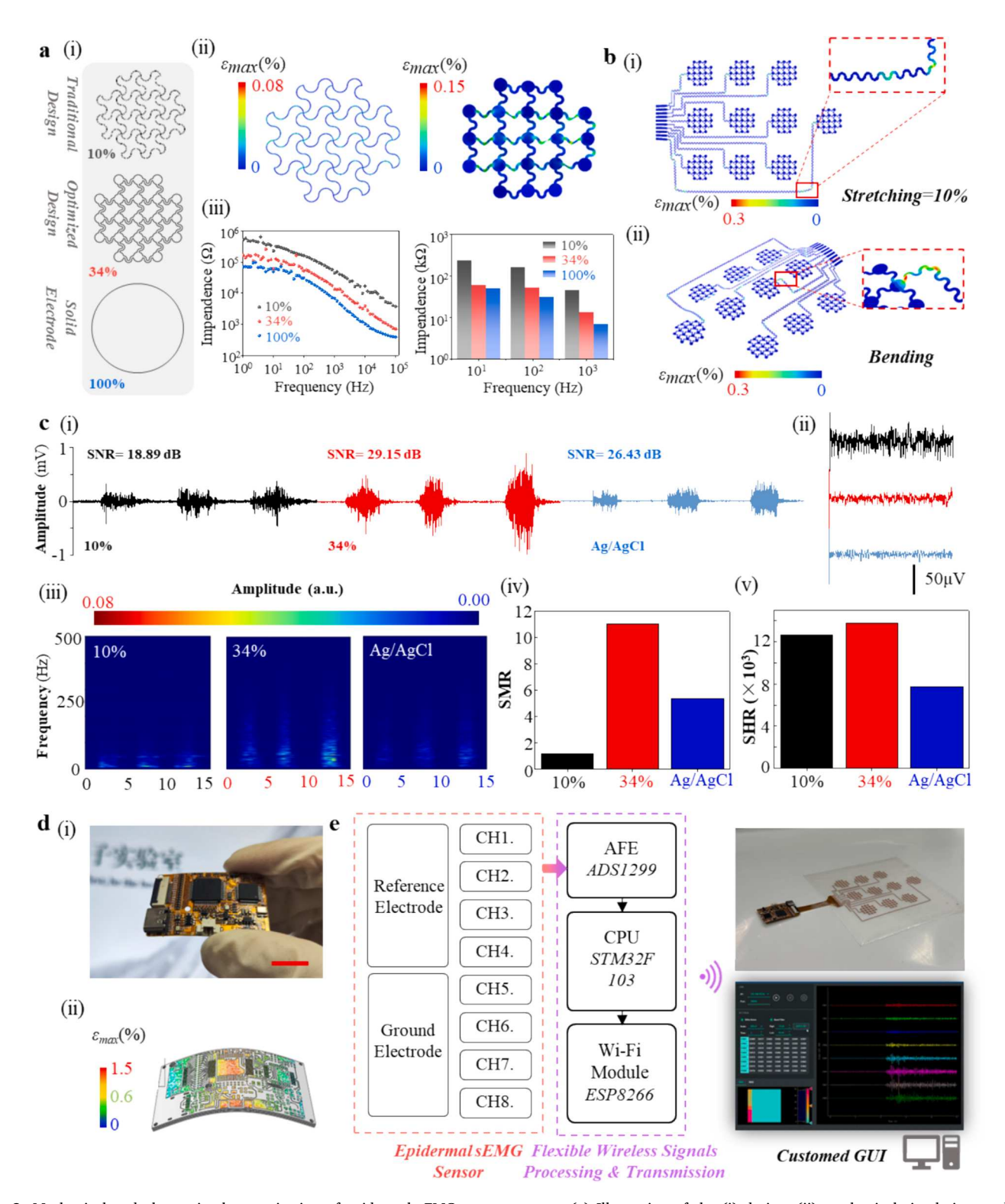


Fig. 3. Mechanical and electronic characterization of epidermal sEMG sensors system. (a) Illustration of the (i) design, (ii) mechanical simulation, and (iii) impedance of the traditional and optimized serpentine epidermal electrode, Ag/AgCl electrode. (b) Simulation results for the deformed geometry and distribution of strain in the copper layer of the epidermal sEMG sensors during uniaxial stretch (~10 %) and bending. (c) (i) EMG signals, (ii) noise baseline, (iii) spectrogram, (iv) SMR, and (v) SHR were measured by traditional (black) and optimized (red) serpentine epidermal electrodes, Ag/AgCl electrode (blue). (d) (i) Photographic image and (ii) mechanical simulation of the fPCB. Scale bar, 1 cm. (e) System-level block diagram showing the signal transduction, processing, and wireless transmission from the sensors to the user interface. (For interpretation of the references to colour in this figure legend, the reader is referred to the web version of this article.)

for achieving the "paste" stage and finish the fabrication of the epidermal sEMG sensors.

Previous studies suggest that the fill factor of the electrode is a noticeable dent in the electrical impedance of the electrode–skin interface, which is the basic requirement for the ability of the electrode to record the EMG signal [35]. As Fig. 2c shows, the traditional serpentine network design with 200 μm linewidth trades off a higher fill factor (fill factor is $\sim\!10$ %) for better stretchability. However, further increasing the width of the serpentine only can slightly improve the fill factor, and the fractal designs (Peano curve, Hilbert curve, et. al) are too complex to design and fabricate. Thus, an easy-to-use optimized design was proposed by appending a solid circle (radius =1 mm) at the intersection of the horizontal and vertical serpentine wires ($\sim\!400~\mu m$), allowing for increasing the fill factor to $\sim\!34$ %.

The stretchable design and multi-layer material strategies of such sensor allow for being directly applied to the skin for real-time surface sEMG signal monitoring without additional adhesives (Fig. 2d), and withstanding skin mechanical deformations (e.g., stretching, and buckling) (Fig. 2d). Moreover, several mini-airholes (~100 μm diameter) were constructed (Fig. 2e and Fig. S4) at the elastomer substrate by a CO₂ laser machine with raster mode (VLS 3.50, Universal) to ensure the great breathability of the sensors. It should be noted that though these mini-airholes are visible, the substrate still maintains good transparency when it interfaces with the skin conformally. As Fig. 2f depicted, its water vapor transmission rate (WVTR, ~ 2.717 mg cm⁻²h⁻¹) is over 6 times higher than that (~0.416 mg cm⁻²h⁻¹) of the substrate without mini-airholes, and is similar to that of an open bottle (~3.287 mg cm⁻²h⁻¹). Conformal contact at the sensor-skin interface is a key factor that has significantly influenced the signal quality [36]. Thus, a model based on the energy-variational method (Supplementary Materials Note 1) was established to understand the relationship between different material strategies with conformal contact [31,36]. The dotted boundary curve shown in Fig. 2g represents the critical points and indicates our proposed epidermal sEMG sensor's properties required for conformal contact. The results verify that the Ecoflex-0030 with Gel 4317 has formed conformal contact with the skin due to the extremely low modulus (~32.23 kPa) and high tackiness (~3.56 N/m). Furthermore, the cytocompatibility test by culturing human lung adenocarcinoma cell line A549 with Ecoflex 0030 and Gel 4317 for 24 h demonstrates healthy growth of the cells and biocompatibility of the elastomer materials (Fig. 2h). There is no sign of skin irritation or allergic reactions as well after using the device on the skin for 12 h (Fig. S5) compared with the traditional Ag/AgCl electrode. With the drastically reduced cost in manufacturing, the low-cost (Table S1) yet high-performance epidermal sEMG sensors promise wide adoption for large-scale application of patients with hand functional movement disorder.

3.2. Mechanical and electrical performance of the fully integrated sEMG system

The stretchability and impedance of these three designs with different fill factors (10 %, 34 %, and 100 %) have been investigated (Fig. 3a). Specifically, the maximum strain in the copper foil in the traditional serpentinite structure is 0.08 % under uniaxial stretching of up to 10 % (with the uniaxial strain of the skin in the target forearm area less than 10 %), which is much lower than the fracture strain of Cu (0.3 %), but the impendence at \sim 1000 Hz is almost double than the solid electrode. The results of the simulation and experiment found clear support that there is still enough stretchability design margin to sacrifice for the lower impedance. Fortunately, finite element analysis (FEA) illustrates the max strain of the Cu in the optimized serpentinite structure is 0.15 % at the elastic stretchability of 10 %, which is sufficient for strains encountered during natural motions of the skin. Moreover, the impedance of the optimized electrode with a fill factor of 34 % is only slightly higher than that of the conductive Ag/AgCl electrode from 1 Hz

to 100 kHz (which is most relevant to EMG signals), and significantly lower than the electrode of traditional serpentine design. Moreover, the simulation result indicates that the single optimized design electrode is employed for the 8-channel epidermal sEMG array inheriting their excellent stretchability (Fig. 3b). Owing to their lower impedance, optimized epidermal electrodes provide high-quality sEMG signals with proven higher SNR (~29.15 dB) compared to traditional serpentine electrodes (~18.89 dB) and standard Ag/AgCl electrodes (~26.43 dB) (Fig. 3c-i), and the amplitude of noise baseline is almost as low as the standard Ag/AgCl electrode (Fig. 3c-ii), which provides evidence of the outstanding conformable and low-impedance property of optimized electrodes. The sEMG signal spectrogram of the traditional design, the optimized design, and the Ag/AgCl standard electrode have been evaluated (Fig. 3c-iii), which revealed that the optimized design electrodes were able to acquire higher energy signals in the critical frequency band of sEMG. Furthermore, the signal-to-motion artifact ratio (SMR) is mainly used to quantitatively assess motion artifacts and is calculated as follows [34]:

$$SMR = \frac{P_{signal}}{P_{0\text{--}20~Hz}}$$

The signal-to-high-frequency noise ratio (SHR) is mainly used to quantify high-frequency noise and is calculated by the formula [34]:

$$SHR = \frac{P_{signal}}{P_{upper20\%}}$$

where P_{signal} denotes the activation signal power, $P_{0-20~Hz}$ denotes the sum of the power densities of the activation signals below 20 Hz, and $P_{upper20\%}$ denotes the sum of the power densities of the activation signals at the higher 20 % of the frequencies. The evaluation of the SMR (Fig. 3c-iv) and SHR (Fig. 3c-v) of these three electrodes reveals that the motion artifacts and high-frequency noise of the electrode with optimized structure design are the lowest, further proving the noise-restrain ability of the electrode with optimized design.

The disposable epidermal array is connected to a reusable flexible printed circuit board (fPCB) (Fig. 3d), and the simulation results indicate that it can ensure bending conformity with the human skin without mechanical failure. In addition, the 8-channel sEMG hardware design comprises MCU, battery, signal analog signal front end (AFE), and Wi-Fi modules (the schematic and PCB diagram are shown in Fig. S6). The system-level block diagram and the circuit diagram (Fig. 3e) illustrate the flow of electrical signals in the sEMG monitoring. A shared top ground electrode and reference electrode facilitate the improvement of the common mode rejection ratio (CMRR) and get high-quality bipolar sEMG signals, the resulting weak biological potential response is amplified and filtered by the signal AFE chip (ADS1299-8, TI). It's worth noting that the ADS1299 outputs 24 bits of data per channel in binary twos complement format with a 24 × amplification factor. After being converted to voltage by a built-in analog-to-digital converter (ADC) with the 500 Hz sampling rate, the acquired data are processed by the MCU chip (STM32F103) and wirelessly transmitted to the user device over Wi-Fi (ESP8266) for further analysis. A self-made graphics user interface (GUI) (Movie S1) is proposed to display and record real-time sEMG waveform and data, and an adjustable bandpass filter is also integrated for further removing noise, the dynamic sEMG maps calculated by root mean square (RMS) provided the spatial and temporal properties of the electrical muscle activity. The overall conformal, soft, breathable, wireless epidermal sEMG sensor system provides a facilitated and precise tool with the clinic application of rehabilitation of hand function.

3.3. Hand gesture recognition by integrated epidermal sEMG system

The hand gesture recognition (HGR) field is of growing interest for hand functional rehabilitation [37–39], motivated by the thirst requirement for both the evaluation of the execution of clinic

K. Yang et al. Materials & Design 243 (2024) 113029

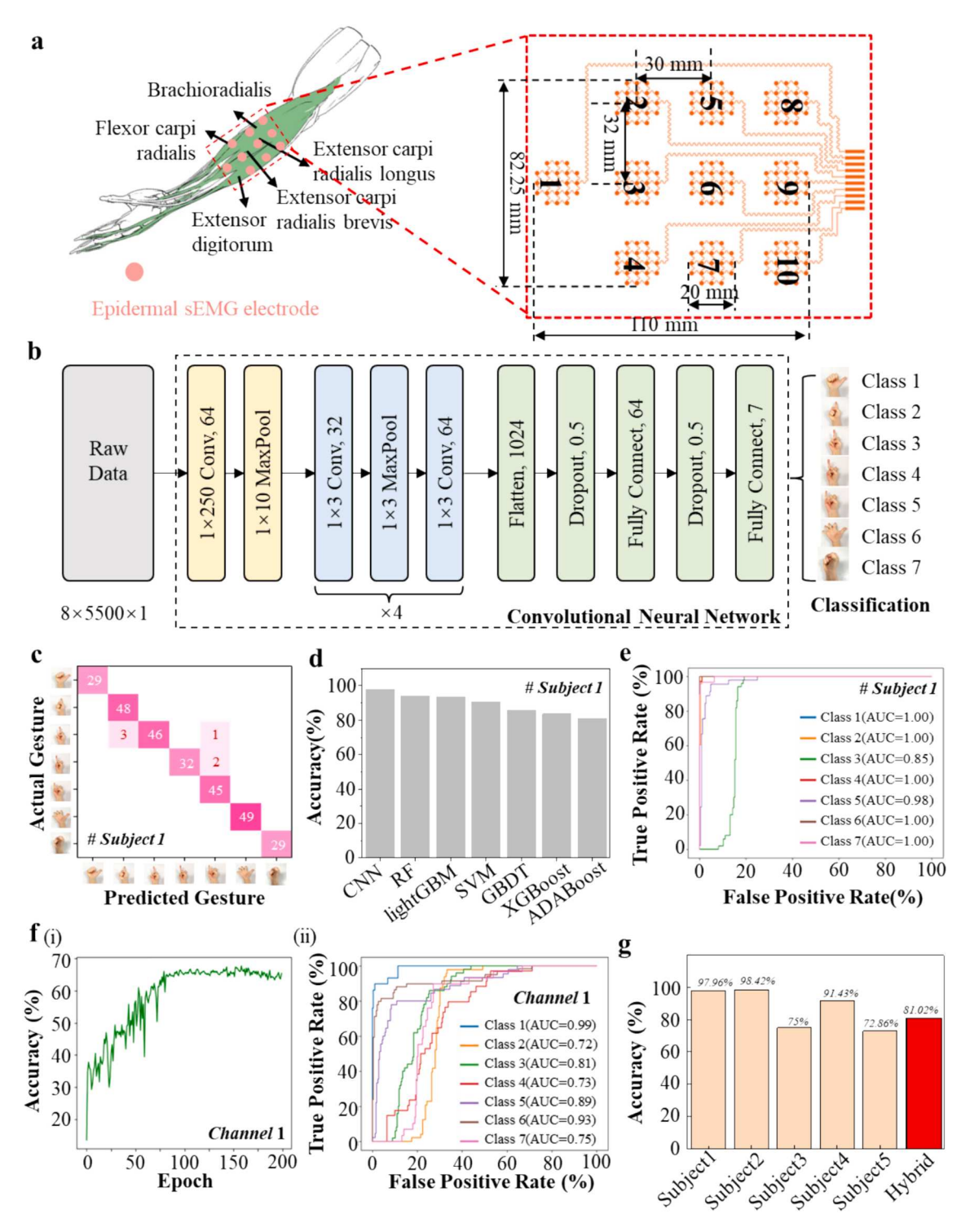


Fig. 4. Hand gesture recognition of the integrated epidermal sEMG sensors system. (a) Schematic illustration of Hand gesture recognition related to forearm superficial muscle groups, and the position of the epidermal sEMG electrode. (b) The architecture of a CNN that takes in sEMG raw data and outputs its probabilities of classes. (c) The confusion matrix of subject 1 from the CNN model. (d) The accuracy of various machine learning models and a CNN model based on the dataset from subject 1. (e) The ROC curves of each classification and the corresponding AUC based on the dataset from subject 1. (f) (i) The accuracy and (ii) ROC curves of each classification and the corresponding AUC based on the dataset from only one channel. (g) The accuracy of HGR based on the dataset from five subjects.

prescription action and the hand motion trajectory prediction for active rehabilitation [40–42]. Such an integrated epidermal sEMG system is applied to monitor sEMG signals by uniform coverage across related forearm superficial muscle groups (Fig. 4a). As Fig. 4a shows, the overall sensor array size is 82.25 mm \times 110 mm, which allows for monitoring brachioradialis, flexor carpi radialis, extensor carpi radialis longus, extensor carpi radialis brevis, and extensor digitorum. There are 14

basic functional movements of the hand including the flexion and extension of five fingers, as well as the flexion, extension, abduction, and adduction of the wrist. As Fig. S7 shows, each movement of a 24-year-old male subject induces a different pattern of EMG signals, and 7 different motion classes (extension of thumb, index finger, middle finger, ring finger, and little finger, as well as the clenching and opening) related rehabilitation have been selected to validate the feasibility of the

integrated epidermal sEMG system for HGR. However, the classification of different hand gestures demands a machine learning model, a 2D deep learning network based on convolutional neural networks (CNN) (Fig. 4b) has been constructed by 8 convolutional layers and 2 fully connected layers with rectified linear unit activation and two dropout layers (p = 0.5) alternately. In addition, the CNN model has been employed and starts with transforming the data format from raw 1D data into a 2D resembling image matrices with shapes of $8\times5500\times1$ for further processing as inputs, and the data through multiple iterations to pass to pooling layers and activation layers to reduce dimensionality, the final fully connected layer of the CNN model has seven neurons with ReLU activation, which corresponds to probabilities associated with the seven types of hand gestures.

There are a total of 1470 pieces of EMG data (class1: 172, class2: 205, class3: 228, class4: 211, class5: 216, class6: 223, class7: 215) in the customized dataset, which are collected by the integrated epidermal sEMG system with a 500 Hz sample rate. Moreover, a high-pass filter (10 Hz) and a notch filter (50 Hz) are utilized to remove the noise. Each

training set consists of a random collection of 80 % of the labeled data, with the remaining 20 % used for validation, and the cross-entropy is employed as the target function for classification. Fig. 4c shows the confusion matrix and demonstrates that the CNN-based deep learning algorithm demonstrates higher prediction accuracy of 97.96 % compared to other commonly used machine learning algorithms (Fig. 4d and Fig. S8), including random forest models, support vector machines, and others. Moreover, the high area under the ROC curve (AUC) is ~ 100 % for five gestures, and the AUC of the middle finger extension gesture classification (class3) is the lowest but still exceeds ~85 %, which indicates that the model achieves a good balance between sensitivity and specificity. However, the accuracy of HGR with only single-channel data (channel 1) drops sharply to ~65 % (Fig. 4f). Since the signal from channel 1 contains information related to the flexor carpi radialis, the recognition accuracy of Class 1 (~99 %) is higher than other gestures, which proves the significance of multi-channel sEMG. Furthermore, the data from the other 4 subjects were collected to expand the dataset, and each person collected 350 sets for seven hand gestures. As Fig. 4g shows,

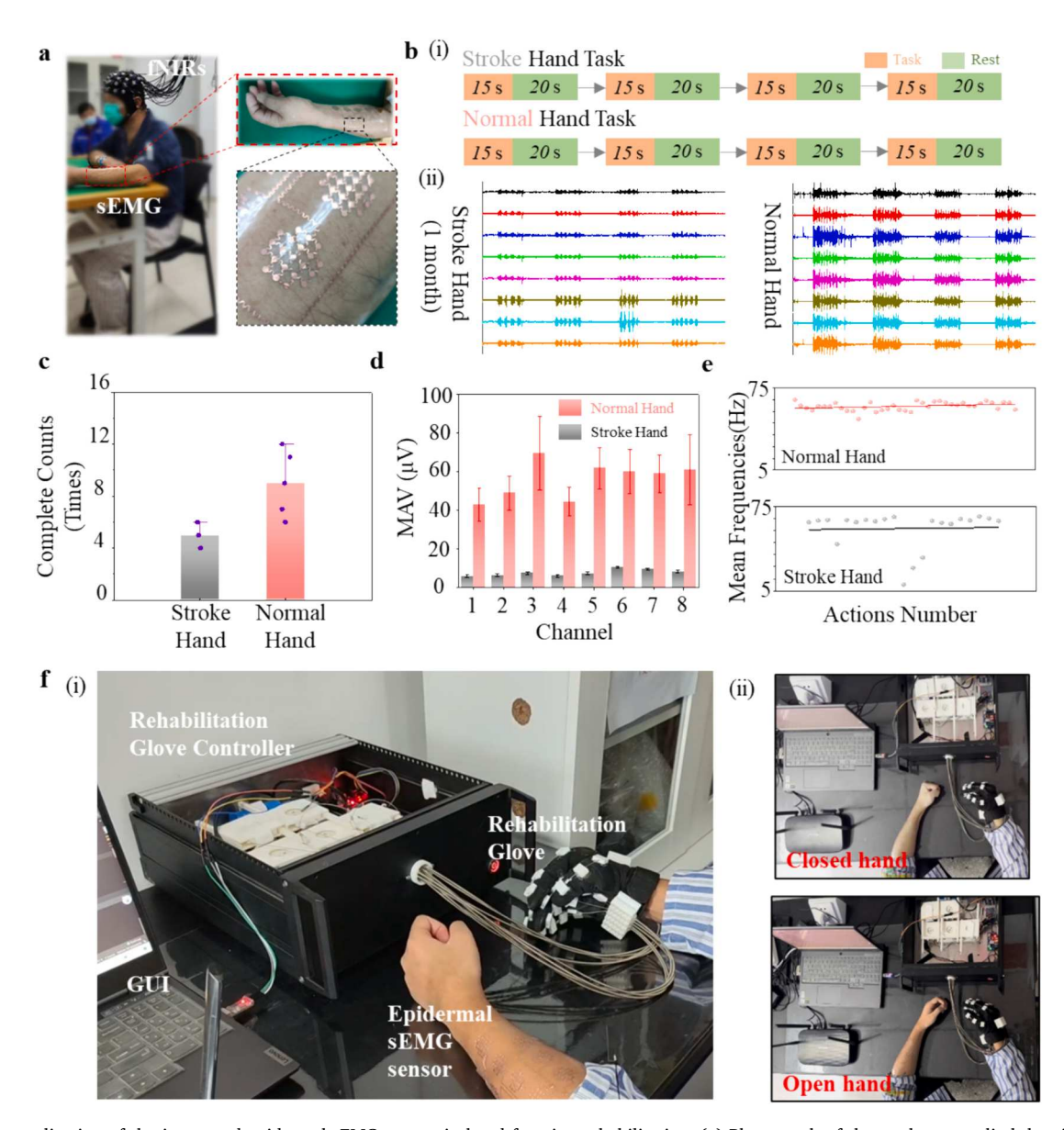


Fig. 5. Clinic application of the integrated epidermal sEMG system in hand function rehabilitation. (a) Photograph of the stroke upper limb hemiplegia patient during grip training. (b) (i) illustration of clinical evaluation setting and (ii) sEMG data recording by the integrated epidermal sEMG system. The comparison of (c) number of complete counts, (d) MAV, and (e) mean frequencies between the intact and affected side hand. (f) (i) Photograph of the MT with the epidermal sEMG sensor for grip exercises and (ii) a session including closed and open affected hand processes.

the accuracy based on the hybrid dataset has declined from 97.96% to 81.02% due to the individual differences in muscle position. It should be noted that optimizing the electrode position based on individual muscle size or increasing the density of the array will help further improve the accuracy. In conclusion, the successful HGR application of our proposed epidermal sEMG system paves the way for further hand function rehabilitation.

3.4. Demonstration of the integrated epidermal sEMG system as a versatile clinical evaluation and control tool

The sEMG can record multiplexed information about stroke patients' muscle and neural recovery activities, and interpretation of the multichannel sEMG data by the feature of time and frequency domains has been widely used for rehabilitation task assessment to dynamic redesign clinical strategies [43-45]. Moreover, the decoding of the patients' hand movement intention can be applied to control rehabilitation robots to achieve active rehabilitation with better treatment effectiveness [46-48]. Compared with the current Ag/AgCl electrodes and fPCBbased electrodes [12,13], our proposed epidermal electrodes are soft, self-adhesive, arrayed, and breathable, which can be distinguished for its conformable, stable, and long-term integration with the skin while preserving the quality of physiological signals despite suffering from the uncontrollable movement and natural sweating. To fully depict its utility as a versatile clinical evaluation and control tool, the epidermal sEMG sensor is applied to the forearm of a postoperative stroke patient (Fig. 5a) who underwent one-month clinic rehabilitation training, to collect sEMG signals from both the intact and affected side during the task formulated by clinic doctors. In particular, the grasp motion is the fundamental behavior according to Brunnstrom's hand function stage (BRS-H) scale [49], and the future daily home-set evaluations should be low-cost and portable. Therefore, the task without other auxiliary equipment revolves around grasp motion as defined by the clinic rehabilitation physician: the subject should repeat the grasp motion as soon as possible during the task time (15 s) for both the intact and affected side, followed by a 20 s rest interval, and considering the patient's physical recovery and fatigue, this task was repeated four times (Fig. 5bi). The sEMG data (Fig. 5b-ii) is successfully recorded with higher SNR and describes the workload-dependent signal amplitude changes for both hands.

The complete counts of the grasp motion during the task period have been calculated through discriminating active segments and relax segments of sEMG based on short-time zero crossing rate autocorrelation measurement, to evaluate the time response ability of neural innervation grasping actions [50,51]. As Fig. 5c shows, the number of grasps on the intact side (\sim 9 times) is higher than on the affected side (\sim 5 times), and the simultaneously tested functional near-infrared spectroscopy (fNIRs) [52,53] of the brain also confirmed that the cerebral blood oxygen activity shows a more disordered status during the stroke hand task period (Fig. S9). Furthermore, the time-domain and frequency-domain characteristics of the sEMG signals under this task were analyzed. Owing to the wide use of mean absolute value (MAV) to reflect the intensity of muscle activation [54], such features has been employed for further analysis. The MAV of each channel for each task period on the intact side was much higher than on the affected side (Fig. 5d), reflecting the faster activation speed, the better recruitment of activated motor units, and the synchronization on the intact side compared to the affected side [55,56]. The integrated EMG (iEMG) can fully reflect the overall EMG output during the concerned period, which can assist the further studies of muscle fatigue, and power output of the stroke patients [57]. The waveform length (WL) includes not only intensity and duration of muscle activation and fatigue status, which is useful for evaluating muscle function and movement control [58]. The features of other time domains (iEMG, WL) (Fig. S9) also exhibit the same trend as the above conclusion. Comparing the changes in mean power frequency (MPF) between the patient's intact and affected sides, no significant differences were observed and indicate that the fatigue degree of the normal hand and stroke hand is the same during the task setting (Fig. 5e) [59,60]. If further information on fatigue level is needed, additional clinic task settings need to be complemented. However, these proof-of-concept clinic experiments have confirmed that the integrated epidermal sEMG system can facilitate the more universal, convenient, and effective assessment of hand function rehabilitation.

Since severe stroke patients can hardly generate strong sEMG signals, mirror therapy (MT) based on the theory of brain function remodeling [61] is a widely used clinical strategy that controls the affected side hand rehabilitation robots by collecting the intention of intact side, creating visual and imagination artifacts of normal hand movement function on the affected side to active the motor cortex of the brain and reduce the degree of the learned non-use. Our integrated epidermal sEMG system has been induced in collaboration with the clinic hand rehabilitation glove for the MT application. Subsequently, the host computer successfully processes the grasping signals to control the commercial rehabilitation glove (EXOduino, Beijing Hangyi Technology Co., Ltd.), and further drives the affected hand in the glove to perform grasping motion (Fig. 5f and Movie S2). We believe in the future, the integrated epidermal sEMG system will have enormous potential to be utilized for more and more hand rehabilitation clinic settings. For instance, the two application scenarios of HGR and positive rehabilitation training can be combined, retraining the CNN model to provide a more intelligent rehabilitation training environment for stroke patients based on mass sEMG signals from clinical stroke patients. Overall, owing to the lost cost and simple fabrication, the overall system can be commercialized and provides a valuable tool for clinical hand rehabilitation assessments and therapy.

4. Conclusion

In summary, a conformal, soft, breathable, wireless epidermal sEMG sensor system has been fabricated by the "laser cut and paste" method to construct the optimized serpentine structures which ensure excellent stretchability and lower "electrode-skin" interface impedance. Such low-cost yet high-performance epidermal electrodes have been employed to hatch 8-channel array sEMG sensors, which during longterm wearing on the skin without any inflammation due to the breathable and biocompatible structure and materials strategies. Moreover, compared with the traditional serpentine and Ag/AgCl electrodes, the self-adhesive property, lower impedance and better conformal contact with skin ensures excellent SNR of the sEMG signals. These remarkable properties of epidermal sEMG sensors integrated with flexible wireless circuits and customized GUI, help us develop a standalone system for hand gesture recognition, clinical evaluation, and therapy. Specifically, with the CNN-based algorithm, the system can automatically and reliably realize the 7 kinds of hand gestures with an accuracy of up to 81.02 %. This tool can be used not only in hand function rehabilitation but also in other human-machine interface applications (prosthetic control [62–64], sign-to-language translation [65–67], virtual reality [68–70], et, al.). More importantly, in clinical scenarios, we have successfully utilized this standalone epidermal system for sEMG evaluation of stroke patients with hand dysfunction, and the easy-to-modify electrode position and low-cost fabrication have enormous potential for other clinical paradigms research. Depending on the information obtained by the sEMG sensors, the integrated systems also be used for controlling the hand rehabilitation glove to realize the mirror therapy. We believe in the future, the integrated epidermal sEMG sensors have enormous potential to provide a remarkable platform for diverse clinical and daily rehabilitation management and therapy scenarios.

CRediT authorship contribution statement

Kerong Yang: Writing – original draft, Software, Methodology, Investigation, Formal analysis, Data curation, Conceptualization.

K. Yang et al. Materials & Design 243 (2024) 113029

Senhao Zhang: Writing - review & editing, Writing - original draft, Validation, Supervision, Software, Resources, Project administration, Methodology, Visualization, Investigation, Funding acquisition, Formal analysis, Data curation, Conceptualization. Ying Yang: Writing - original draft, Validation, Project administration, Methodology, Investigation, Conceptualization. Xiaoman Liu: Writing - original draft, Supervision, Resources, Methodology, Investigation, Formal analysis, Data curation. Jiuqiang Li: Writing - original draft, Software, Resources, Methodology, Data curation. Benkun Bao: Writing - original draft, Software, Resources, Methodology, Data curation. Chang Liu: Writing - original draft, Supervision, Resources, Methodology, Formal analysis. Hongbo Yang: Writing - review & editing, Visualization, Validation, Supervision, Methodology, Funding acquisition, Formal analysis, Conceptualization. Kai Guo: Writing - review & editing, Writing - original draft, Software, Resources, Funding acquisition, Formal analysis, Data curation. Huanyu Cheng: Writing - review & editing, Writing - original draft, Visualization, Validation, Supervision, Software, Resources, Project administration, Methodology, Investigation, Funding acquisition, Formal analysis, Data curation, Conceptualization.

Declaration of competing interest

The authors declare that they have no known competing financial interests or personal relationships that could have appeared to influence the work reported in this paper.

Data availability

Data will be made available on request.

Acknowledgments

S.Z. acknowledges the support provided by the National Natural Science Foundation of China (Grant No. 62301556), the Key Research and Development Program of Jiangsu Province (Grant No. BE2021012-1), the Shandong Natural Science Foundation (ZR2023QH203), excellent postdoctoral fellows of Jiangsu province, and also would like to acknowledge Qi Lu's love and parents' support. K.G. acknowledges the support provided by the National Key R&D Program of China (2023YFB4706203), the Shandong Natural Science Foundation (ZR2022QH214). H.C. acknowledges the support provided by NIH (Award No. R21EB030140), NSF (Grant Nos. 2309323 and 2319139), and Penn State University.

Appendix A. Supplementary data

Supplementary data to this article can be found online at https://doi.org/10.1016/j.matdes.2024.113029.

References

- [1] L Liu, W Chen, H Zhou, et al., Chinese Stroke Association guidelines for clinical management of cerebrovascular disorders: executive summary and 2019 update of clinical management of ischaemic cerebrovascular diseases, Stroke Vasc. Neurol. 5.2(2020).
- [2] C.O. Johnson, M. Nguyen, G.A. Roth, et al., Global, regional, and national burden of stroke, 1990–2016: a systematic analysis for the Global Burden of Disease Study 2016. Jancet Neurol. 18 (5) (2019) 439–458.
- [3] M.A. Delph, S.A. Fischer, P.W. Gauthier, et al., editors. A soft robotic exomusculature glove with integrated sEMG sensing for hand rehabilitation, in: 2013 IEEE 13th International Conference on Rehabilitation Robotics (ICORR); 2013: IEEE.
- [4] J Lobo-Prat, P N Kooren, A H Stienen, et al., Non-invasive control interfaces for intention detection in active movement-assistive devices, J. Neuroeng. Rehabil., 11 (1) (2014) 1–22
- [5] J. Rosen, M. Brand, M.B. Fuchs, et al., A myosignal-based powered exoskeleton system, IEEE Trans. Syst. Man Cybern.-Part A: Syst. Hum. 31(3) (2001) 210–222.
- [6] M.H. Rahman, C. Ochoa-Luna, M. Saad, EMG based control of a robotic exoskeleton for shoulder and elbow motion assist, (2015).

[7] R. Gopura, K. Kiguchi, Electromyography (EMG)-signal based fuzzy-neuro control of a 3 degrees of freedom (3DOF) exoskeleton robot for human upper-limb motion assist, 37(4) (2009).

- [8] D. Farina, R. Merletti, R.M. Enoka, The extraction of neural strategies from the surface EMG: an update, J. Appl. Physiol. 117 (11) (2014) 1215–1230.
- [9] Y. Nam, B. Koo, A. Cichocki, et al., GOM-Face: GKP, EOG, and EMG-based multimodal interface with application to humanoid robot control, IEEE Trans. Biomed. Eng. 61 (2) (2013) 453–462.
- [10] M.J. Hong, J.B. Park, Y.J. Lee, et al., Quantitative evaluation of post-stroke spasticity using neurophysiological and radiological tools: a pilot study, Ann. Rehab. Med. 42 (3) (2018) 384–395.
- [11] Y.H. Yin, Y.J. Fan, L.D. Xu, EMG and EPP-integrated human "machine interface between the paralyzed and rehabilitation exoskeleton, IEEE Trans. Inf Technol. Biomed. 16 (4) (2012) 542–549.
- [12] S.H. Yeon, T. Shu, H. Song, et al., Acquisition of surface EMG using flexible and low-profile electrodes for lower extremity neuroprosthetic control, IEEE Trans. Med. Rob. Bionics, 3 (3) (2021) 563–572.
- [13] Y. Li, H. Pan, Q. Song, editors. ADS1299-Based Array Surface Electromyography Signal Acquisition System. Journal of Physics: Conference Series (2022).
- Signal Acquisition System. Journal of Physics: Conference Series (2022). [14] C. Connolly, Prosthetic hands from touch bionics, Ind. Rob. 35 (4) (2008) 290–293.
- [15] Q. Ding, J. Han, X. Zhao, Continuous estimation of human multi-joint angles from sEMG using a state-space model, IEEE Trans. Neural Syst. Rehab. Eng. 25 (9) (2016) 1518–1528.
- [16] R. Chen, A. Canales, P. Anikeeva, Neural recording and modulation technologies, Nat. Rev. Mater. 2 (2) (2017) 1–16.
- [17] S. Liu, D.S. Shah, R. Kramer-Bottiglio, Highly stretchable multilayer electronic circuits using biphasic gallium-indium, Nat. Mater. 20 (6) (2021) 851–858.
- [18] Y.J. Hong, H. Jeong, K.W. Cho, et al., Wearable and implantable devices for cardiovascular healthcare: from monitoring to therapy based on flexible and stretchable electronics, Adv. Funct. Mater. 29 (19) (2019) 1808247.
- [19] D.-H. Kim, N. Lu, R. Ma, et al., Epidermal electronics, Science, 333 (6044) (2011) 838–843.
- [20] S. Huang, Y. Liu, Y. Zhao, et al., Flexible electronics: stretchable electrodes and their future, Adv. Funct. Mater. 29 (6) (2019) 1805924.
- [21] V. Toral, E. Castillo, A. Albretch, et al., Cost-effective printed electrodes based on emerging materials applied to biosignal acquisition, IEEE Access 8 (2020) 127789–127800.
- [22] J. Xu, S. Wang, G.-J.-N. Wang, et al., Highly stretchable polymer semiconductor films through the nanoconfinement effect, Science 355 (6320) (2017) 59-64.
- [23] S Wang, J Xu, W Wang, et al., Skin electronics from scalable fabrication of an intrinsically stretchable transistor array, Nat. Commun., 555 (7694) (2018) 83–88.
- [24] Y.S. Zhang, A. Khademhosseini, Advances in engineering hydrogels, Science 356 (6337) (2017) 3627.
- [25] S. Xu, Y. Zhang, L. Jia, et al., Soft microfluidic assemblies of sensors, circuits, and radios for the skin, Science, 344 (6179) (2014) 70–74.
- [26] C. Wang, C. Wang, Z. Huang, et al., Materials and structures toward soft electronics, Adv. Mater. 30 (50) (2018) 1801368.
- [27] S.M. Won, E. Song, J. Zhao, et al., Recent advances in materials, devices, and systems for neural interfaces, Adv. Mater. 30 (30) (2018) 1800534.
- [28] Y. Yang, Y. Song, X. Bo, et al., A laser-engraved wearable sensor for sensitive detection of uric acid and tyrosine in sweat, Nat. Biotechnol., 38 (2) (2020) 217–224.
- [29] J.-W. Jeong, W.-H. Yeo, A. Akhtar, et al., Materials and optimized designs for human-machine interfaces via epidermal electronics, Adv. Mater. 25 (47) (2013).
- [30] K.-I. Jang, S.Y. Han, S. Xu, et al., Rugged and breathable forms of stretchable electronics with adherent composite substrates for transcutaneous monitoring, Nat. Commun., 5(1) (2014) 4779.
- [31] S. Wang, M. Li, J. Wu, et al., Mechanics of epidermal electronics, Science (2012).
- [32] S. Yang, Y.C. Chen, L. Nicolini, et al., manufacture of multiparametric epidermal sensor systems, Adv. Mater. 27 (41) (2015) 6423–6430.
- [33] R. Pilkar, K. Momeni, A. Ramanujam, et al., Use of surface EMG in clinical rehabilitation of individuals with SCI: barriers and future considerations, Front. Neurol., 11 (2020) 578559.
- [34] J. Chang, A. Phinyomark, E. Scheme, editors. Assessment of EMG benchmark data for gesture recognition using the NinaPro database. 2020 42nd Annual International Conference of the IEEE Engineering in Medicine & Biology Society (EMBC); 2020: IEEE.
- [35] S. Wang, Y. Huang, J.A. Rogers, Mechanical designs for inorganic stretchable circuits in soft electronics, IEEE Trans. Compon. Packag. Manuf. Technol. 5 (9) (2015) 1201–1218.
- [36] Y.S. Kim, M. Mahmood, Y. Lee, et al., All-in-one, wireless, stretchable hybrid electronics for smart, connected, and ambulatory physiological monitoring, Adv. Sci. 6 (17) (2019) 1900939.
- [37] W.-J. Li, C.-Y. Hsieh, L.-F. Lin, et al., editors. Hand gesture recognition for poststroke rehabilitation using leap motion, in: 2017 international conference on applied system innovation (ICASI); 2017: IEEE.
- [38] M. Wu, Gesture recognition based on deep learning: A review, EAI Endors. Trans. e-Learn. 10 (2024).
- [39] R. Tchantchane, H. Zhou, S. Zhang, et al., A review of hand gesture recognition systems based on noninvasive wearable sensors, Adv. Intell. Syst. 5 (10) (2023) 2300207.
- [40] V. Gohel, N. Mehendale, Review on electromyography signal acquisition and processing, Biophys. Rev. 12 (6) (2020) 1361–1367.
- 41] S. Jiang, P. Kang, X. Song, et al., Emerging wearable interfaces and algorithms for hand gesture recognition: A survey, IEEE Rev. Biomed. Eng. 15 (2021) 85–102.

- [42] S. Cai, Y. Chen, S. Huang, et al., SVM-based classification of sEMG signals for upper-limb self-rehabilitation training, Front. Neurorob., 13 (2019) 31.
- [43] Y. Zhou, Y. Fang, K. Gui, et al., sEMG bias-driven functional electrical stimulation system for upper-limb stroke rehabilitation, IEEE Sens. J. 18 (16) (2018) 6812–6821
- [44] C. Lambelet, M. Lyu, D. Woolley, et al., editors. A wearable wrist exoskeleton with sEMG-based force control for stroke rehabilitation, in: 2017 International Conference on Rehabilitation Robotics (ICORR); 2017: IEEE.
- [45] K. Ma, Y. Chen, X. Zhang, et al., sEMG-based trunk compensation detection in rehabilitation training, Front. Neurosci. 13 (2019) 1250.
- [46] M. Jochumsen, I.K. Niazi, M Zia ur Rehman, et al., Decoding attempted hand movements in stroke patients using surface electromyography, Sensors, 20 (23) (2020) 6763.
- [47] A Ramos-Murguialday, E Garca-Cossio, A Walter, et al., Decoding upper limb residual muscle activity in severe chronic stroke, Ann. Clin. Transl. Neurol., 2 (1) (2015) 1–11
- [48] O.W. Samuel, M.G. Asogbon, Y. Geng, et al., Decoding movement intent patterns based on spatiotemporal and adaptive filtering method towards active motor training in stroke rehabilitation systems, Neural Comput. Appl. 33 (2021) 4703–4806
- [49] S. Brunnstrom, Motor testing procedures in hemiplegia: based on sequential recovery stages, Phys. Ther., 46 (4) (1966) 357–375.
- [50] H.K. Hameed, W.Z. Hasan, S. Shafie, et al., editors. An amplitude independent muscle activity detection algorithm based on adaptive zero crossing technique and mean instantaneous frequency of the sEMG signal, in: 2017 IEEE Regional Symposium on Micro and Nanoelectronics (RSM); 2017: IEEE.
- [51] I. Conradsen, S.N. Beniczky, K. Hoppe, et al., Automated algorithm for generalized tonic-clonic epileptic seizure onset detection based on sEMG zero-crossing rate, IEEE Trans. Biomed. Eng., 59 (2) (2011) 579–585.
- [52] C. Huo, Z. Sun, G. Xu, et al., fNIRS-based brain functional response to robotassisted training for upper-limb in stroke patients with hemiplegia, Front. Aging Neurosci. 14 (2022) 1060734.
- [53] S.B. Lim, S. Peters, C.-l. Yang, et al., Frontal, sensorimotor, and posterior parietal regions are involved in dual-task walking after stroke, Front. Neurol. 13 (2022) 904145
- [54] J. Park, H. Park, J. Kim, Performance estimation of the lower limb exoskeleton for plantarflexion using surface electromyography (sEMG) signals, J. Biomech. Sci. Eng., 12 (2) (2017) 16-00595-00516-00595.
- [55] Z. Fan, C. Zhao, L. Luo, et al., editors. Study on sEMG-based exercise therapy for upper limb of severe hemiplegic patients, in: 2013 35th Annual International Conference of the IEEE Engineering in Medicine and Biology Society (EMBC); 2013: IEEE.

- [56] H.M. James, N.V. Iqbal, Review on feature extraction and classification of neuromuscular disorders, Int. J. Mod. Trends Sci. Technol., (2019) 2455-3778.
- [57] L. Ren, C. Nie, S. Li, et al., Analysis of sEMG signal and its application in rehabilitation medicine, Информационные техно (2018) 364–368.
- [58] P. Qin, X. Shi, Evaluation of feature extraction and classification for lower limb motion based on sEMG signal, Entropy 22 (8) (2020) 852.
- [59] R. Merletti, S. Roy, Myoelectric and mechanical manifestations of muscle fatigue in voluntary contractions, J. Orthop. Sports Phys. Ther. 24 (6) (1996) 342–353.
- [60] A.F. Mannion, P. Dolan, A. Mannion, et al., Relationship between myoelectric and mechanical manifestations of fatigue in the quadriceps femoris muscle group, Eur. J. Appl. Physiol. Occup. Physiol., 74 (1996) 411–419.
- [61] K.N. Arya, Underlying neural mechanisms of mirror therapy: Implications for motor rehabilitation in stroke, Neurol. India 64 (1) (2016) 38.
- [62] F. Palermo, M. Cognolato, A. Gijsberts, et al., editors. Repeatability of grasp recognition for robotic hand prosthesis control based on sEMG data, in: 2017 International Conference on Rehabilitation Robotics (ICORR); (2017): IEEE.
- [63] J. Park, J. Jeong, M. Kang, et al., Imperceptive and reusable dermal surface EMG for lower extremity neuro-prosthetic control and clinical assessment, npj Flex. Electron., 7 (1) (2023) 49.
- [64] D.V. Anaya, M.R. Yuce, Forearm Dual-Triboelectric Sensor (FDTS) for assistive Human-Machine-Interfaces (HMIs) and robotic control with potential uses in prosthetic devices, Nano Energy 111 (2023) 108366.
- [65] K.R. Pyun, K. Kwon, M.J. Yoo, et al., Machine-learned wearable sensors for realtime hand motion recognition: toward practical applications in reality, Natl. Sci. Rev. 298 (2023).
- [66] Y. Gu, C. Zheng, M. Todoh, et al., American sign language translation using wearable inertial and electromyography sensors for tracking hand movements and facial expressions, Front. Neurosci. 16 (2022) 962141.
- [67] E. Pereira-Montiel, E. Pérez-Giraldo, J. Mazo, et al., Automatic sign language recognition based on accelerometry and surface electromyography signals: A study for Colombian sign language, Biomed. Signal Process. Control 71 (2022) 103201.
- [68] X. Li, Z. Zhou, W. Liu, et al., Wireless sEMG-based identification in a virtual reality environment, Microelectron. Reliab. 98 (2019) 78–85.
- [69] C.L. Toledo-Peral, G. Vega-Martínez, J.A. Mercado-Gutiérrez, et al., Virtual/ augmented reality for rehabilitation applications using electromyography as control/biofeedback: systematic literature review, Electronics 11 (14) (2022) 2271
- [70] T.S. Castañeda, M. Connan, P. Capsi-Morales, et al., Experimental evaluation of the impact of sEMG interfaces in enhancing embodiment of virtual myoelectric prostheses, J. Neuroeng. Rehab., 21 (1) (2024) 1–16.